Computer Physics Communications 180 (2009) 854–860

Contents lists available at ScienceDirect

Computer Physics Communications

www.elsevier.com/locate/cpc

Efficiently computing vortex lattices in rapid rotating Bose–Einstein condensates

Rong Zeng [a], Yanzhi Zhang [b,*]

[a] Department of Electrical Engineering, Tsinghua University, Beijing, 100084, China
[b] Department of Mathematics, National University of Singapore, Singapore 117543

ARTICLE INFO

Article history:
Received 21 March 2008
Received in revised form 24 November 2008
Accepted 2 December 2008
Available online 7 December 2008

PACS:
11.10.Jj
11.10.St
31.15.-p

Keywords:
Rotating Bose–Einstein condensate
Gross–Pitaevskii equation
Vortex lattices
Strong repulsive interaction regime
Angular momentum rotation

ABSTRACT

We propose an efficient and spectrally accurate numerical method for computing vortex lattices in rapid rotating Bose–Einstein condensates (BECs), especially with strong repulsive interatomic interaction. The key ingredient of this method is to discretize the normalized gradient flow by Fourier spectral method in space and by semi-implicit Euler method in time. Different vortex lattice structures of condensate ground states in two-dimensional (2D) and 3D rapid rotating BECs are reported for both harmonic and harmonic-plus-quartic potentials. In addition, vortex lattices in rotating BECs with optical lattice potentials are also presented.

1. Introduction

Gaseous Bose–Einstein condensates (BECs) offer a versatile testing ground for the study of superfluidity where quantized vortices play an important role. The first observation of a single vortex line was in weakly interacting alkali gases by using the Reman transition phase-printing method [1,2]. Multiply charged vortices were also created by using the topological phase engineering method [3]. Recently, vortex lattices containing more than one hundred vortices were observed by rotating the condensate with a laser spoon [4–7]. It is expected that more complicated vortex clusters can be created in the future, and such states would enable various opportunities, ranging from investigating the properties of random polynomials [8] to using vortices in quantum memories [9]. In addition, recent experimental developments enable one to create a confinement potential either tighter than a harmonic potential or as an optical lattice, which opens possible methods to explore the nature of BECs with/without the oscillating potential. All these developments spur great interests in the study of vortex lattice structures of condensate ground state in rapid rotating BECs with strong repulsive interaction.

There are many different numerical methods proposed in the literature to compute the stationary state of non-rotating and rotating BECs. For example, an imaginary time method was used in [10,11] for finding ground states of BECs, a hybrid three steps Runge–Kutta–Crank–Nicolson scheme was proposed in [12,13] for computing S-shape or U-shape vortex lines in 3D BECs, an adaptive step-size Runge–Kutta finite difference method was applied in [14,15] for studying the nucleation of vortex arrays in rotating anisotropic BECs, and a backward Euler finite difference method was proposed in [16,17] for computing ground states of non-rotating and rotating BECs. More approaches can be found in [18–24] and references therein. In all the above methods, the second- or fourth-order compact finite difference scheme is used to discretize space derivatives. Due to the finite order accuracy (usually second-order, fourth-order or even sixth-order) of the spatial discretization, these methods have difficulties to get the accurate results in rapid rotating BECs, especially with strong repulsive interaction. Because in this case, very complicated vortex lattice structures may appear in the condensate [25–27], and the high spatial resolution of the numerical method is strongly demanded.

In this paper, we present an efficient and spectrally accurate numerical method to compute vortex lattices of condensate ground state in rapid rotating BECs, especially when the interatomic interaction is strongly repulsive. This method discretizes the normalized gradient flow, also known as the Gross–Pitaevskii equation (GPE) in the imaginary time, by Fourier spectral method for spatial deriva-

* Corresponding author. Current address: Department of Scientific Computing, Florida State University, Tallahassee, FL 32306-4120, USA.
E-mail addresses: zengrong@tsinghua.edu.cn (R. Zeng), yzhang5@fsu.edu (Y. Zhang).

0010-4655/$ – see front matter
doi:10.1016/j.cpc.2008.12.003

tives and backward Euler scheme for time derivatives. The fast direct Poisson solver is applied to solve the large linear system at each time step, and also the stabilization technique is used such that the time step can be chosen as large as possible [28]. Vortex lattice structures of condensate ground state are reported in the 2D and 3D rapid rotating BECs with different external potentials. We obtain results in the strong interacting regime which are not reported in the literature. In addition, we also compute vortex lattices of rotating BEC with optical lattice potentials not reported before. In fact, our preliminary aim of the paper is not to find new physics, but to propose an efficient and most accurate numerical method for computing vortex lattices of condensate ground state in rapid rotating BECs.

This paper is organized as follows. In Section 2 we introduce the model under the investigation and discuss different trapping potentials. In Section 3 the numerical methods are introduced in detail. Vortex lattices of condensate ground state in 2D and 3D rotating BECs are reported in Sections 4 and 5, respectively. Finally, we make the conclusions in Section 6.

2. The Gross–Pitaevskii equation

At temperatures T much smaller than the critical temperature T_c [29], a rotating BEC trapped in an external potential can be described by a macroscopic wave function $\psi(\mathbf{x},t)$ which obeys the Gross–Pitaevskii equation (GPE). In the rotating frame with a frequency Ω around the z-axis, the GPE reads

$$i\hbar\frac{\partial\psi(\mathbf{x},t)}{\partial t}=\left[-\frac{\hbar^2}{2m}\nabla^2+V_{\mathrm{trap}}(\mathbf{x})+g|\psi|^2-\Omega L_z\right]\psi(\mathbf{x},t),\quad t\geqslant 0,\tag{2.1}$$

where $\mathbf{x}=(x,y,z)^T\in\mathbb{R}^3$ is the spatial coordinate vector, $\hbar$ is the Planck constant, m is the atomic mass, $g=4\pi\hbar^2a_s/m$ represents the strength of the interaction between particles with a_s (positive for repulsive interaction and negative for attractive interaction) the s-wave scattering length, and $L_z=-i\hbar(x\partial_y-y\partial_x)$ is the z-component of the angular momentum. $V_{\mathrm{trap}}(\mathbf{x})$ is a real-valued external potential whose shape is determined by the type of system under investigations, and if the harmonic trapping potential is considered, it has the form

$$V_{\mathrm{trap}}(\mathbf{x})=\frac{m}{2}\left(\omega_x^2x^2+\omega_y^2y^2+\omega_z^2z^2\right),\tag{2.2}$$

where ω_x, ω_y and ω_z are the trapping frequencies in x-, y-, and z-direction, respectively. The wave function is normalized by

$$\int_{\mathbb{R}^3}\left|\psi(\mathbf{x},t)\right|^2d\mathbf{x}=N,\quad t\geqslant 0\tag{2.3}$$

with N the total number of atoms.

For the numerical purpose, it is convenient to rescale the spatial and temporal variables. By assuming $\omega_x=\min\{\omega_x,\omega_y,\omega_z\}$ and introducing

$$\mathbf{x}=a_0\tilde{\mathbf{x}},\qquad t=\frac{\tilde{t}}{\omega_x},\qquad \Omega=\omega_x\tilde{\Omega},\qquad \psi=\frac{\sqrt{N}\tilde{\psi}}{a_0^{3/2}}\tag{2.4}$$

with $a_0=\sqrt{\hbar/2m\omega_x}$, the GPE (2.1) can be reduced to the following dimensionless form (removing $\tilde{}$ for simplicity):

$$i\frac{\partial\psi(\mathbf{x},t)}{\partial t}=\left[-\frac{1}{2}\nabla^2+V_3(\mathbf{x})+\beta_3\left|\psi(\mathbf{x},t)\right|^2-\Omega L_z\right]\psi(\mathbf{x},t),\tag{2.5}$$

where $\beta_3=4\pi Na_s/a_0$ and $L_z=-i(x\partial_y-y\partial_x)$. The dimensionless harmonic potential takes the form

$$V_3(\mathbf{x})=\frac{1}{2}\left(x^2+\gamma_y^2y^2+\gamma_z^2z^2\right)\tag{2.6}$$

with $\gamma_y=\omega_y/\omega_x$ and $\gamma_z=\omega_z/\omega_x$. The wave function satisfies that

$$\int_{\mathbb{R}^3}\left|\psi(\mathbf{x},t)\right|^2d\mathbf{x}=1,\quad t\geqslant 0.\tag{2.7}$$

Furthermore, if it is tightly confined in the axial direction, i.e. $\gamma_z\gg 1$ and $\gamma_y=O(1)$, the dynamics of a BEC can be well approximated by the 2D GPE under the normalization (2.7) [12,16]:

$$i\partial_t\psi(\mathbf{x},t)=\left[-\frac{1}{2}\nabla^2+V_2(\mathbf{x})+\beta_2\left|\psi(\mathbf{x},t)\right|^2-\Omega L_z\right]\psi(\mathbf{x},t)\tag{2.8}$$

with $\mathbf{x}=(x,y)^T\in\mathbb{R}^2$, and

$$V_2(\mathbf{x})=\frac{1}{2}\left(x^2+\gamma_y^2y^2\right),\qquad \beta_2\approx\beta_3\sqrt{\frac{\gamma_z}{2\pi}}.$$

In recent experiments, other potentials are also applied to study the behavior of rapid rotating BECs. For example, the harmonic-plus-quartic potential has the form [25,30,31]

$$V_d(\mathbf{x})=\begin{cases}(1-\alpha)r^2+\kappa r^4, & d=2,\\ (1-\alpha)r^2+\kappa r^4+\gamma_z^2z^2, & d=3,\end{cases}\tag{2.9}$$

where $r=\sqrt{x^2+y^2}$, and α, κ and γ_z are positive constants; the harmonic-plus-optical lattice potential reads [23]

$$V_d(\mathbf{x})=\begin{cases}\frac{1}{2}(x^2+y^2+V_{\mathrm{opt}}), & d=2,\\ \frac{1}{2}(x^2+y^2+\gamma_z^2z^2+V_{\mathrm{opt}}), & d=3,\end{cases}\tag{2.10}$$

where $V_{\mathrm{opt}}(x,y)=V_0(\sin^2(\kappa x)+\sin^2(\kappa y))$ is the optical lattice potential with V_0 and κ two positive constants.

The ground state solution $\phi_g(\mathbf{x})$ of the d-dimensional ($d=2,3$) GPE is defined as which minimizes the Gross–Pitaevskii energy

$$E_{\beta_d,\Omega}(\phi)=\int_{\mathbb{R}^d}\left[\frac{1}{2}|\nabla\phi|^2+V_d(\mathbf{x})|\phi|^2+\frac{\beta_d}{2}|\phi|^4-\Omega\,\mathrm{Re}(\phi^*L_z\phi)\right]d\mathbf{x},\tag{2.11}$$

and satisfies the normalization constraint

$$\int_{\mathbb{R}^d}\left|\phi(\mathbf{x})\right|^2d\mathbf{x}=1,\tag{2.12}$$

where f^* and $\mathrm{Re}(f)$ denote the conjugate and the real part of the function f, respectively.

3. Numerical methods

In the literature (see, e.g. [17,23,28]), the minimizer of $E_{\beta_d,\Omega}(\phi)$ was found by applying an imaginary time (i.e. $t\to -it$) in the GPE and evolving a gradient flow with discrete normalization [16]. In this section, we will first introduce the normalized gradient flow under the rotational frame and then present spectral type methods to discretize it.

3.1. Normalized gradient flow

Choose a time step $\Delta t>0$ and define the time sequence $t_n=n\Delta t$ for $n=0,1,\ldots$. For each time interval $[t_n,t_{n+1})$, the gradient flow (or called as the GPE in imaginary time) has the form [12,16]

$$\partial_t\phi(\mathbf{x},t)=\left[\frac{1}{2}\nabla^2-V_d(\mathbf{x})-\beta_d\left|\phi(\mathbf{x},t)\right|^2+\Omega L_z\right]\phi(\mathbf{x},t),\tag{3.13}$$

which also can be viewed as applying the steepest decent method to the energy functional (2.11). To satisfy the normalization (2.12), at the end of each step the solution is projected back to the unit sphere, i.e., letting

$$\phi(\mathbf{x}, t_{n+1}) = \frac{\phi(\mathbf{x}, t_{n+1})}{\|\phi(\cdot, t_{n+1})\|}$$

$$\text{with} \quad \|\phi(\cdot, t_{n+1})\|^2 = \int_{\mathbb{R}^d} |\phi(\mathbf{x}, t_{n+1})|^2 \, d\mathbf{x}. \tag{3.14}$$

The initial condition for (3.13) is given by

$$\phi(\mathbf{x}, 0) = \phi_0(\mathbf{x}) \quad \text{with} \int_{\mathbb{R}^d} |\phi_0(\mathbf{x})|^2 \, d\mathbf{x} = 1. \tag{3.15}$$

It was proven that when $\beta_d = 0$, $\Omega = 0$ and $V_d(\mathbf{x}) \geqslant 0$, the normalized gradient flow (3.13)–(3.15) is energy diminishing for any time step $\Delta t > 0$ and any initial data $\phi_0(\mathbf{x})$ [16,28].

3.2. Semi-implicit Euler spectral discretization

For simplicity, the numerical method is introduced only for the 2D case, and its generalization to 3D case is straightforward. Due to the external trapping potential, e.g., (2.6), (2.9) and (2.10), the solution of (3.13)–(3.15) decays to zero exponentially fast when $|\mathbf{x}| \to \infty$. Thus in practical computations, we can truncate the problem into a bounded computational domain $\Omega_{\mathbf{x}} = [a, b] \times [c, d]$ with homogeneous Dirichlet boundary conditions, where $|a|$, b, $|c|$ and d are sufficiently large to ensure that the effect of the truncated boundary can be neglected.

Choose mesh sizes $\Delta x = (b - a)/M > 0$ and $\Delta y = (d - c)/N > 0$ with M and N two even positive integers. Denote grid points

$$x_j = a + j\Delta x, \qquad y_k = c + k\Delta y,$$

for $j = 0, 1, \ldots, M$ and $k = 0, 1, \ldots, N$. Let $\phi^n_{j,k}$ be the numerical approximation of $\phi(x_j, y_k, t_n)$ and ϕ^n be the solution vector with components $\phi^n_{j,k}$. Then the semi-implicit Euler Fourier pseudospectral discretization for (3.13) with $d = 2$ can be given by

$$\frac{\phi^*_{j,k} - \phi^n_{j,k}}{\Delta t} = \left(\frac{1}{2}\nabla^2_h - V_2(x_j, y_k) - \beta_2 |\phi^n_{j,k}|^2 + \Omega L_h\right)\phi^*_{j,k} \tag{3.16}$$

for $1 \leqslant j \leqslant M - 1$ and $1 \leqslant k \leqslant N - 1$, where ∇^2_h and L_h, the pseudospectral differential operators approximating the operators ∇^2 and L_z, respectively, are defined as [32]

$$\nabla^2_h \phi^*_{j,k} = -\sum_{p=-M/2}^{M/2-1} \sum_{q=-N/2}^{N/2-1} (\mu_p^2 + \lambda_q^2)\widehat{\phi^*_{p,q}} e^{i\frac{2jp\pi}{M}} e^{i\frac{2kq\pi}{N}},$$

$$L_h \phi^*_{j,k} = (x_j D^h_y - y_k D^h_x)\phi^*_{j,k},$$

$$D^h_x \phi^*_{j,k} = \sum_{p=-M/2}^{M/2-1} \sum_{q=-N/2}^{N/2-1} \mu_p \widehat{\phi^*_{p,q}} e^{i\frac{2jp\pi}{M}} e^{i\frac{2kq\pi}{N}},$$

$$D^h_y \phi^*_{j,k} = \sum_{p=-M/2}^{M/2-1} \sum_{q=-N/2}^{N/2-1} \lambda_q \widehat{\phi^*_{p,q}} e^{i\frac{2jp\pi}{M}} e^{i\frac{2kq\pi}{N}}$$

with

$$\widehat{\phi^*_{p,q}} = \frac{1}{MN} \sum_{j=0}^{M-1} \sum_{k=0}^{N-1} \phi^*_{j,k} e^{-i\frac{2jp\pi}{M}} e^{-i\frac{2kq\pi}{N}},$$

$$\mu_p = \frac{2p\pi}{b-a}, \qquad \lambda_q = \frac{2q\pi}{d-c},$$

for $p = -M/2, \ldots, M/2 - 1$ and $q = -N/2, \ldots, N/2 - 1$. In addition, the projection step (3.14) and the initial condition (3.15) can be discretized, respectively, as

$$\phi^{n+1}_{j,k} = \frac{\phi^*_{j,k}}{\|\phi^*\|} \quad \text{with } \|\phi^*\|^2 = \Delta x \Delta y \sum_{j=1}^{M-1} \sum_{k=1}^{N-1} |\phi^*_{j,k}|^2, \tag{3.17}$$

$$\phi^0_{j,k} = \phi_0(x_j, y_k), \quad j = 0, 1, \ldots, M, \ k = 0, 1, \ldots, N. \tag{3.18}$$

In the discretization (3.16), at each time step, a linear system has to be solved. Here it is solved iteratively by introducing a stabilization term with constant coefficients [28], i.e.,

$$\frac{\phi^{*,m+1}_{j,k} - \phi^n_{j,k}}{\Delta t} = \left(\frac{1}{2}\nabla^2_h - \alpha\right)\phi^{*,m+1}_{j,k} + G^m_{j,k}, \tag{3.19}$$

where m defines the iteration step, the term

$$G^m_{j,k} = \left(\alpha - V_2(x_j, y_k) - \beta_2 |\phi^n_{j,k}|^2 + \Omega L_h\right)\phi^{*,m}_{j,k},$$

and $\alpha \geqslant 0$ is the stabilization parameter chosen as $\alpha = \frac{1}{2}(b_{\max} + b_{\min})$ with

$$b_{\max} = \max_{j,k}\left(V_2(x_j, y_k) + \beta_2 |\phi^n_{j,k}|^2\right),$$

$$b_{\min} = \min_{j,k}\left(V_2(x_j, y_k) + \beta_2 |\phi^n_{j,k}|^2\right).$$

Taking the discrete Fourier transform at both sides of (3.19), we obtain

$$\frac{\widehat{\phi^{*,m+1}_{p,q}} - \widehat{\phi^n_{p,q}}}{\Delta t} = -\left(\alpha + \frac{1}{2}(\mu_p^2 + \lambda_q^2)\right)\widehat{\phi^{*,m+1}_{p,q}} + \widehat{G^m_{p,q}}.$$

Solving the above equation, we get

$$\widehat{\phi^{*,m+1}_{p,q}} = \frac{2}{2 + \Delta t(2\alpha + \mu_p^2 + \lambda_q^2)}\left(\widehat{\phi^n_{p,q}} + \Delta t\, \widehat{G^m_{p,q}}\right),$$

for $p = -M/2, \ldots, M/2 - 1$ and $q = -N/2, \ldots, N/2 - 1$.

3.3. Backward/forward Euler spectral discretization

In practice, in order to avoid solving the linear system (3.19) iteratively, one can also use the backward/forward Euler scheme for linear/nonlinear terms in time derivatives, i.e. the gradient flow (3.13) can be discretized as

$$\frac{\phi^*_{j,k} - \phi^n_{j,k}}{\Delta t} = \frac{1}{2}\nabla^2_h \phi^*_{j,k} - \left(V_2(x_j, y_k) + \beta_2 |\phi^n_{j,k}|^2 - \Omega L_h\right)\phi^n_{j,k}, \tag{3.20}$$

for $1 \leqslant j \leqslant M - 1$ and $1 \leqslant k \leqslant N - 1$.

Similarly, to efficiently solve (3.20), a stabilization term α can be introduced, and at each time step the resulting linear system is solved by the direct Poisson solver via discrete fast Fourier transform. Thus the memory cost is $O(MN)$ and the computational cost per time step is $O(MN \ln(MN))$.

4. Numerical results in 2D

In this section, we report numerical results for vortex lattices of condensate ground state in 2D rotating BEC with strong repulsive interaction and different external potentials. The converged solution of the normalized gradient flow (3.13)–(3.15) is obtained by requiring that

$$\max_{j,k} \frac{|\phi^{n+1}_{j,k} - \phi^n_{j,k}|}{\Delta t} < \varepsilon = 10^{-6}. \tag{4.1}$$

Different initial data $\phi_0(\mathbf{x})$ in (3.15) are tested in order to trigger the lowest energy of the converged solution [16,28]. In general, we choose $\phi_0(\mathbf{x})$ as a superposition of the ground state and a central vortex state with winding number $m = 1$ of non-rotating BEC which has the same interaction strength as that used in (3.13) [16,28]. The computational domain is chosen as a square $\Omega_{\mathbf{x}} = [-16, 16] \times [-16, 16]$. A refined grid with 513×513 nodes is used, and our numerical experiments show that it is sufficient to achieve grid independent solutions. The time step is chosen as $\Delta t = 0.005$.

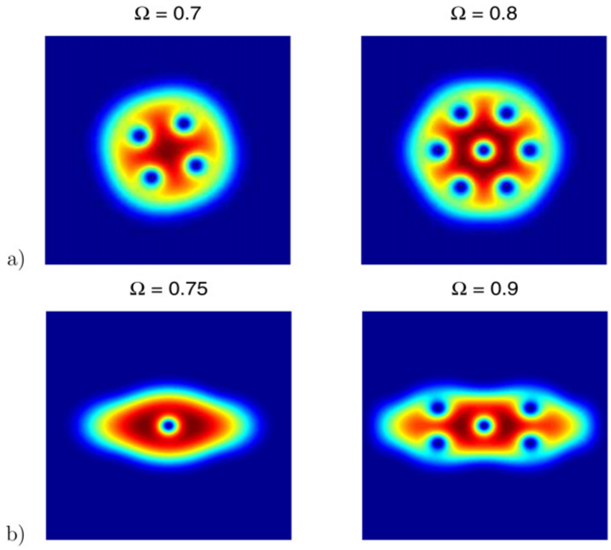

Fig. 1. Vortex lattices of condensate ground state in rotating BECs with a harmonic potential and $\beta_2 = 100$. a) Symmetric trap with $\gamma_y = 1$; b) asymmetric trap with $\gamma_y = 1.5$.

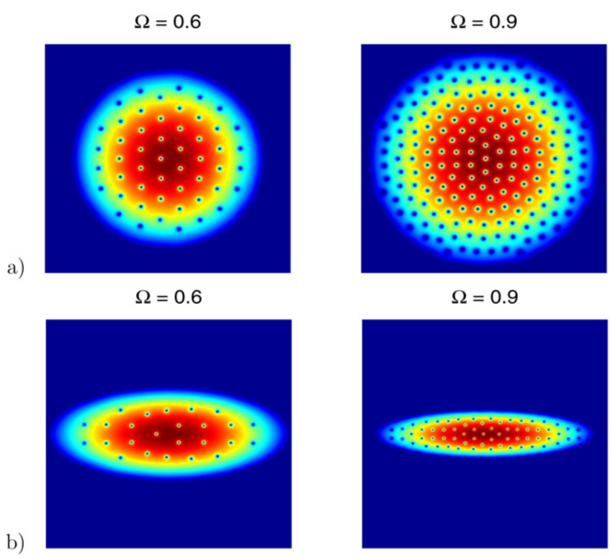

Fig. 2. Vortex lattices of condensate ground state in rotating BECs with a harmonic potential and strong repulsive interaction $\beta_2 = 8000$. a) Symmetric trap with $\gamma_y = 1$; b) asymmetric trap with $\gamma_y = 2$.

4.1. For harmonic potential

In rotating BECs with a harmonic potential, the condensate ground state exists only when $|\Omega| < \gamma_{\min} := \min\{1, \gamma_y\}$ [12,16]. If $|\Omega| > \gamma_{\max} := \max\{1, \gamma_y\}$, there is no ground state because in this case the centrifugal force caused by the angular rotation is very large, so that it can compensate the trapping force and prevent the condensate from creating a stable state. Without loss of generality, we assume that $\gamma_y \geqslant 1$ and study the case of $\Omega < 1$ in the following computations.

Figs. 1–2 display vortex lattice structures of condensate ground state for different parameters Ω, β_2 and γ_y. We find that the ground state in a harmonic potential is a triangular lattice composed of a number of single vortices with winding number $m = 1$, which confirms the theoretical prediction in [33]. The number of vortices depends on the parameters β_2, Ω and γ_y. For fixed γ_y, the increase either in β_2 or in $|\Omega|$ will cause more vortices in the lattice. On the other hand, for fixed β_2 and Ω, the larger the frequency γ_y, the smaller the number of vortices. Also, we find that the number of vortices in a symmetric potential (i.e. $\gamma_y = 1$) is much larger than that in an asymmetric potential (i.e. $\gamma_y \neq 1$).

In addition, with the increasing of the number of vortices, the lattice becomes much denser, and thus to capture the feature of each vortex, the spatial resolution must be high enough. Due to its spectral accuracy in space, our methods can resolve the lattice structures very well. While the low-order finite difference methods have difficulties, especially in the regime of strong repulsive interaction [25].

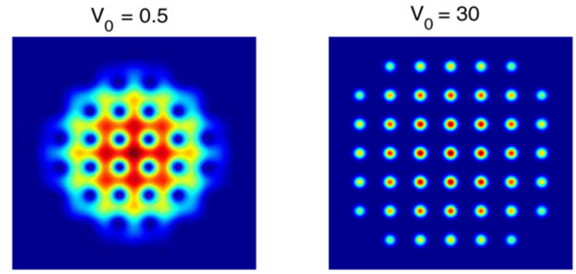

Fig. 3. Vortex lattices of condensate ground state in rotating BECs with a harmonic-plus-optical lattice potential for $d = 2$ and $\kappa = \frac{\pi}{2}$ in (2.10).

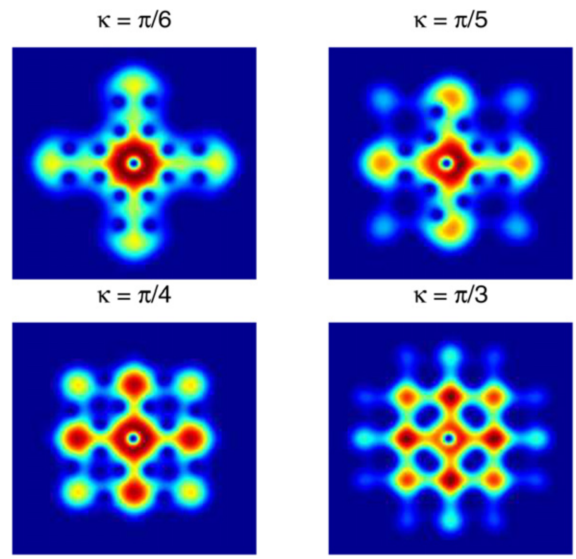

Fig. 4. Vortex lattices of condensate ground state in rotating BECs with a harmonic-plus-optical lattice potential for $d = 2$ and $V_0 = 2.5$ in (2.10).

4.2. For harmonic-plus-optical lattice potential

To study the condensate ground state of rotating BEC with an oscillating potential, we use a harmonic-plus-optical lattice potential defined in (2.10). Figs. 3–4 show the numerical results for $\beta_2 = 200$ and $\Omega = 0.9$.

From Fig. 3, we see that if κ is fixed and V_0 is small, the vortex lattice is of square structure, which is different from that in the harmonic potential (cf. Figs. 1 and 2). When V_0 becomes large, there is no vortex in the condensate ground state any more because of the strong confinement of the optical wells. Fig. 4 shows that for small and fixed V_0, the condensate ground state is a vortex lattice having many single vortices located in the optical wells. With κ increasing, the effect of the optical lattice becomes insignificant, and eventually when κ becomes large enough, the condensate ground state in a harmonic-plus-optical lattice potential has the similar structure to that in a harmonic potential.

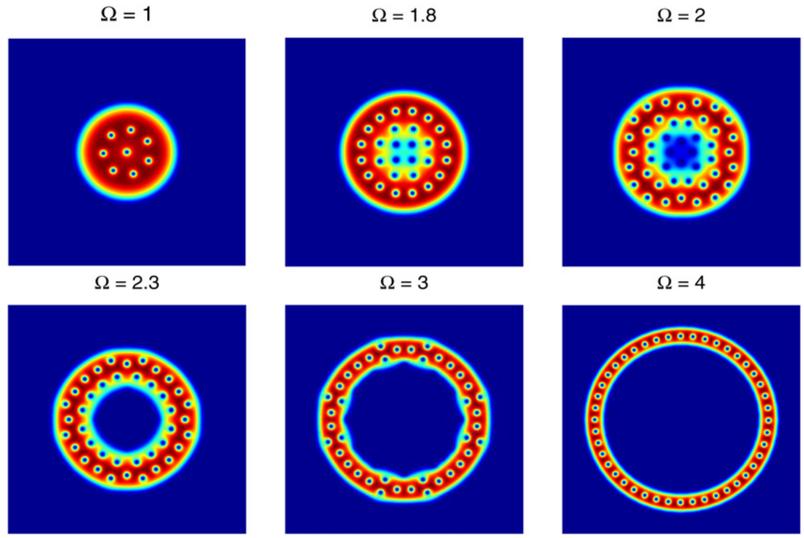

Fig. 5. Vortex lattices of condensate ground state in rapid rotating BECs with a harmonic-plus-quartic potential and $\beta_2 = 1000$.

4.3. For harmonic-plus-quartic potential

As mentioned in Section 4.2, the harmonic potential is not tight enough when the rotational speed Ω becomes very large. Thus to study the condensate ground state in rapid rotating BECs, one possible way is to apply a stiffer potential, e.g., the harmonic-plus-quartic potential in (2.9).

For $\beta_2 = 1000$, Fig. 5 shows the numerical results in a harmonic-plus-quartic potential with $\alpha = 1.2$ and $\kappa = 0.3$, and Fig. 6 plots the energy $E_{\beta_2,\Omega}(\phi)$ and angular momentum expectation $\langle L_z\rangle(\phi)$ of the condensate ground state versus the rotation speed Ω, where the angular momentum expectation is defined as

$$\langle L_z\rangle(\phi) = \int_{\mathbb{R}^2} \phi^* L_z \phi \, d\mathbf{x} = i \int_{\mathbb{R}^2} \phi^* (y\partial_x - x\partial_y)\phi \, d\mathbf{x}. \tag{4.2}$$

From them, we see that for small Ω, the condensate ground state is a vortex lattice having many single vortices. With the increase of Ω, the number of vortices increases, but the density at the condensate center decreases very fast. When the rotating speed Ω becomes large enough, the atoms are completely 'thrown' out of the center due to the large centrifugal force, so that the density at the condensate center becomes zero. Thus in this case, the condensate ground state is a giant 'hole' surrounded by a number of single vortices (cf. Fig. 5). If the speed Ω increases further, both the size of the hole and the number of single vortices increase. However, the width of the annulus containing single vortices becomes smaller because of the competition between the forces from the angular rotation and the potential confinement.

In addition, Fig. 7 depicts numerical results for strong repulsive interaction case with $\beta_2 = 10\,000$. Comparing Figs. 5 and 7, we find that the larger β_2 can introduce much more vortices in the condensate ground state, which makes the density of the lattice very large. Again, in this case the high spatial resolutions are strongly demanded.

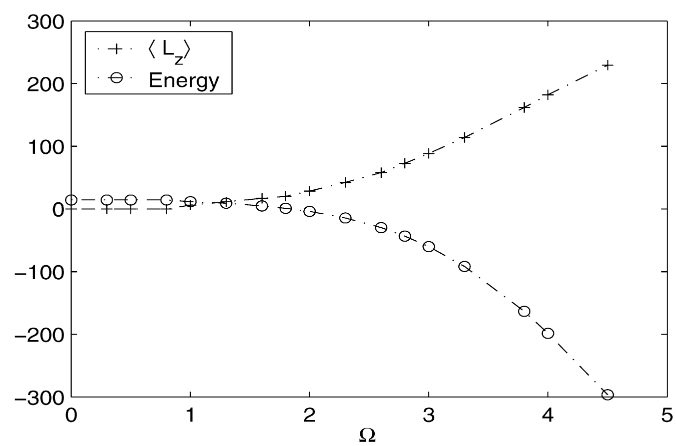

Fig. 6. Energy and angular momentum expectation of condensate ground state versus rotating speed Ω when $\beta_2 = 1000$.

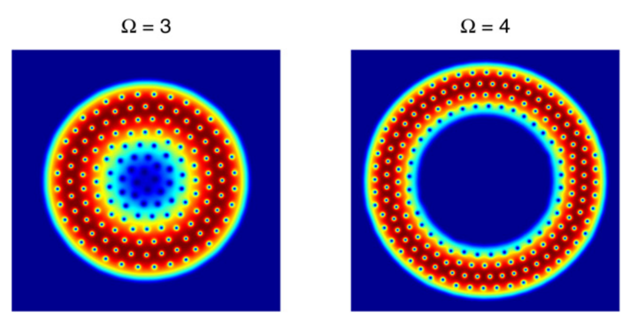

Fig. 7. Vortex lattices of condensate ground state in rapid rotating BEC with a harmonic-plus-quartic potential and $\beta_2 = 10\,000$.

Fig. 8 shows the time evolution of the density $|\phi|$. From it, we see that during the time evolution, the boundary of the condensate becomes unstable, and the density at the condensate center decreases very fast to be zero. As a result, a central 'ring' with high density is formed at time $t = 0.24$. At the same time, a number of vortices enter the ring from both the inner and outer boundaries. With the increase of the vortex number, the repulsive interactions between vortices become significant, which push the vortices apart from the each other. Eventually, the competition between the rotating force and the interacting force makes a stable vortex lattice which is a critical point of the energy functional $E_{\beta_2,\Omega}(\phi)$ in (2.11).

4.4. Dynamics of the normalized gradient flow

In order to know the formation of vortex lattices, in this section we study the time evolution of the normalized gradient flow (3.13)–(3.15). A harmonic-plus-quartic potential with $\alpha = 1.2$ and $\kappa = 0.3$ is applied, and the other parameters are set as $\beta_2 = 1000$ and $\Omega = 2.5$. The initial data $\phi_0(\mathbf{x})$ in (3.15) is chosen as the Thomas–Fermi approximate state [23].

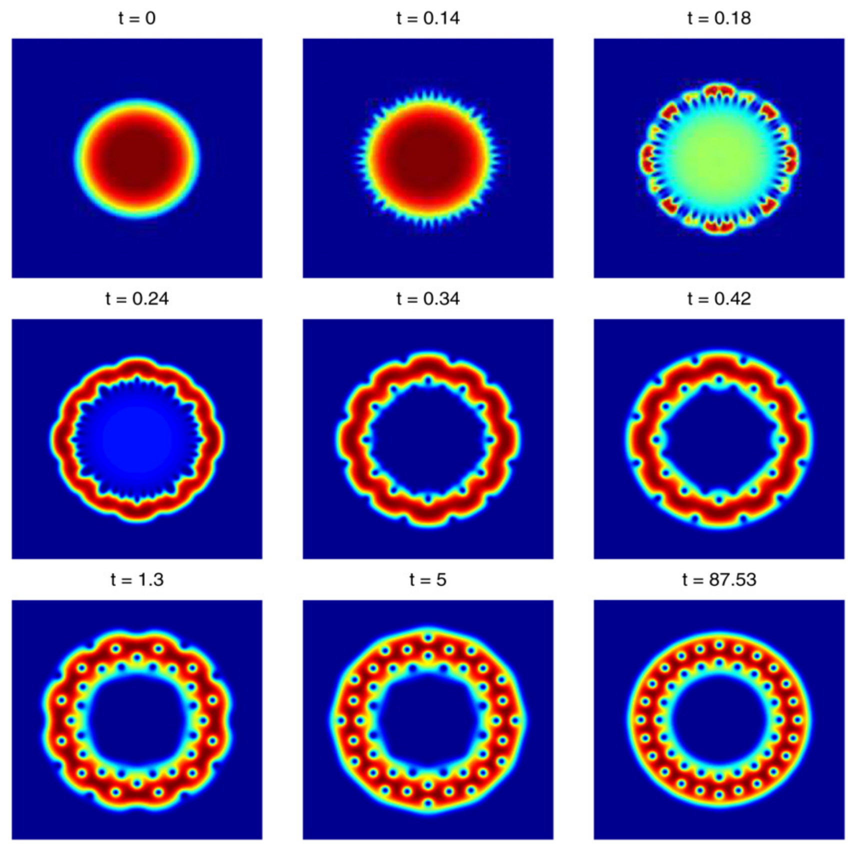

Fig. 8. Contour plots of the density $|\phi|$ in time evolution of the normalized gradient flow (3.13)–(3.15) to show the formation of vortex lattices in a harmonic-plus-quartic potential.

In addition, Fig. 9 shows time evolution of the energy $E_{\beta_2,\Omega}(\phi)$ and the angular momentum expectation $\langle L_z\rangle(\phi)$ for time $t \in [0, 3]$. After time $t = 3$, the changes on both of them are slight, so we omit the plot for $t \in [3, 87.53]$ for simplicity. From Fig. 9, we find that in a short time, i.e. $t \in [0, 0.5]$, the energy decreases and the angular momentum expectation increases dramatically because of the appearance of a large number of vortices. After it, they evolve slowly which corresponds to the rearrangement of the vortices.

5. Numerical results in 3D

In this section, we report numerical results for 3D rotating BECs with strong repulsive interaction. Similar to the 2D case, the initial data in (3.15) is taken as a superposition of the ground state and a central vortex line of non-rotating BECs. The computational domain is defined in a box $\Omega_{\mathbf{x}} = [-8, 8] \times [-8, 8] \times [-8, 8]$. A refined grid with $257 \times 257 \times 129$ nodes is used, which is sufficient to obtain grid independent solutions. The time step is chosen as $\Delta t = 0.01$.

Fig. 10 shows 3D vortex lattices of condensate ground state in a symmetric harmonic potential with $\gamma_y = \gamma_z = 1$ and $\beta_3 = 400$. From it and our additional computations not shown here, we find that the ground state in 3D rotating BECs is composed of parallel vortex lines. Increasing in either β_3 or Ω can cause more vortex lines generated into the condensate.

Fig. 11 displays the numerical results in 3D rotating BECs with a harmonic-plus-quartic potential, where the parameters are chosen as $\alpha = 1.2$, $\kappa = 0.3$, $\gamma_z = 1$ and $\beta_3 = 100$. Similar to the 2D case, when the rotation speed is very large, the density at the condensate center becomes zero, so that a giant ‘hole’ appears at the center. There exists a critical rotation speed $\Omega_{cr}(\beta_3, \alpha, \kappa)$. If $\Omega > \Omega_{cr}(\beta_3, \alpha, \kappa)$ but close to the critical rotation speed, the ground state is composed of a giant hole surrounded by many single vortex lines, e.g., the case of $\Omega = 1.4$ in Fig. 11. When Ω becomes much larger than $\Omega_{cr}(\beta_3, \alpha, \kappa)$, single vortex lines disappear and only a big hole is left at the center of the condensate; see Fig. 11 with $\Omega = 1.8$.

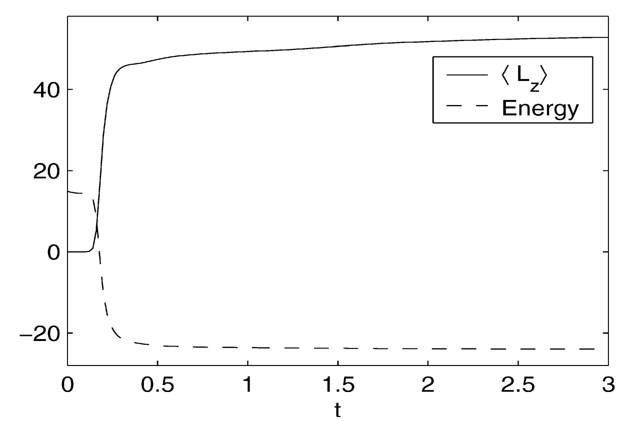

Fig. 9. Time evolution of the energy $E_{\beta_2,\Omega}(\phi)$ and the angular momentum expectation $\langle L_z\rangle(\phi)$ of the normalized gradient flow (3.13)–(3.15).

6. Conclusion

We developed an efficient method to compute vortex lattices of condensate ground state in rapid rotating BECs. This method has spectral accuracy in space, so it can be used especially for the strong repulsive interaction regime which is never reached by the standard finite difference methods proposed in the literature. The condensate ground states in 2D rotating BECs were studied in detail for different external trapping potentials. In addition, the 3D results were also presented for harmonic and harmonic-plus-

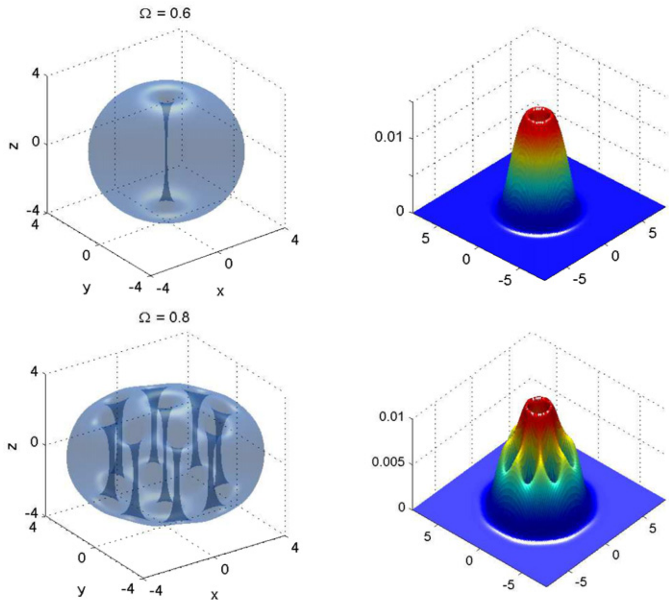

Fig. 10. Isosurface plots (left) and surface plots at $z = 0$ (right) for the vortex lattices of condensate ground state in 3D rotating BECs with a harmonic potential and $\beta_3 = 400$.

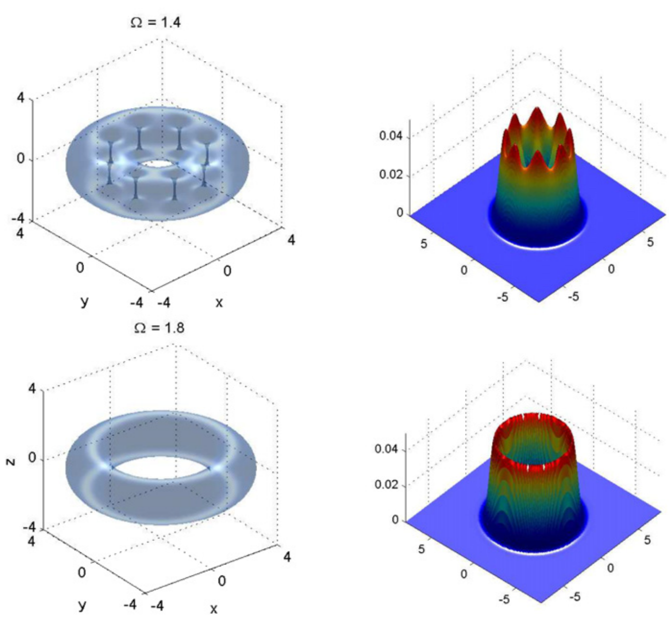

Fig. 11. Isosurface plots (left) and surface plots at $z = 0$ (right) for the vortex lattices of condensate ground state in 3D rotating BECs with a harmonic-plus-quartic potential with $\beta_3 = 100$.

quartic potentials. Some conclusions were drawn from our numerical results.

In a harmonic potential, the vortex lattice of condensate ground state is of the triangular structure, and it is composed of many single vortices. It was found that for a fixed rotation speed Ω, the lattice in a symmetric potential (i.e. $\gamma_y = \gamma_x = 1$) contains more vortices than that in an asymmetric potential with $\gamma_y > \gamma_x = 1$. This is because in an asymmetric potential, the tighter confinement in one direction prevents the creation of vortices in that direction. The vortex lattice in the harmonic-plus-optical lattice is more complicated, and it depends on the height of optical wells and also on the distance between two neighboring wells.

The structure of vortex lattices in rapid rotating BECs with harmonic-plus-quartic potential is much different from that in a harmonic potential. For large rotation speed Ω, the density at the condensate center is zero and the condensate ground state is an annulus containing a number of vortices. The larger the rotation speed Ω, the smaller the width of the annulus.

Acknowledgement

We thank helpful discussions with Professor Weizhu Bao in the subject. Y. Zhang acknowledges support from Singapore Ministry of Education grant No. R-146-000-083-112. This work was partially done while the second author was visiting the Institute for Mathematical Sciences, National University of Singapore, in 2007.

References

[1] M.R. Matthews, B.P. Anderson, P.C. Haljan, D.S. Hall, C.E. Wieman, E.A. Cornell, Phys. Rev. Lett. 83 (1999) 2498.
[2] P.C. Haljan, I. Coddington, P. Engels, E.A. Cornell, Phys. Rev. Lett. 87 (2001) 210403.
[3] A.E. Leanhardt, A. Görlitz, A.P. Chikkatur, D. Kielpinski, Y. Shin, D.E. Pritchard, W. Ketterle, Phys. Rev. Lett. 89 (2002) 190403.
[4] K.W. Madison, F. Chevy, W. Wohlleben, J. Dalibard, Phys. Rev. Lett. 84 (2000) 806.
[5] K.W. Madison, F. Chevy, W. Wohlleben, J. Dalibard, J. Mod. Opt. 47 (2000) 2715.
[6] J.R. Abo-Shaeer, C. Raman, J.M. Vogels, W. Ketterle, Science 292 (2001) 476.
[7] C. Raman, J.R. Abo-Shaeer, J.M. Vogels, K. Xu, W. Ketterle, Phys. Rev. Lett. 87 (2001) 210402.
[8] Y. Castin, Z. Hadzibabic, S. Stock, J. Dalibard, S. Stringari, Phys. Rev. Lett. 96 (2006) 040405.
[9] K.T. Kapale, J.P. Dowling, Phys. Rev. Lett. 95 (2005) 173601.
[10] M.L. Chiofalo, S. Succi, M.P. Tosi, Phys. Rev. E 62 (2000) 7438.
[11] F. Dalfovo, S. Giorgini, L.P. Pitaevskii, S. Stringari, Rev. Mod. Phys. 71 (1999) 463.
[12] A. Aftalion, Q. Du, Phys. Rev. A 64 (2001) 063603.
[13] A. Aftalion, T. Riviere, Phys. Rev. A 64 (2001) 043611.
[14] D.L. Feder, C.W. Clark, B.I. Schneider, Phys. Rev. A 61 (1999) 011601.
[15] D.L. Feder, A.A. Svidzinsky, A.L. Fetter, C.W. Clark, Phys. Rev. Lett. 86 (2001) 564.
[16] W. Bao, Q. Du, SIAM J. Sci. Comput. 25 (2004) 1674.
[17] W. Bao, P.A. Markowich, H. Wang, Comm. Math. Sci. 3 (2005) 57.
[18] M. Edwards, K. Burnett, Phys. Rev. A 51 (1995) 1382.
[19] R.J. Dodd, J. Res. Natl. Inst. Stand. Technol. 101 (1996) 545.
[20] B. Jackson, J.F. McCann, C.S. Adams, Phys. Rev. Lett. 80 (1998) 3903.
[21] J.J. García-Ripoll, V.M. Pérez-García, Phys. Rev. A 63 (2001) 041603.
[22] W. Bao, W. Tang, J. Comput. Phys. 187 (2003) 230.
[23] W. Bao, F.Y. Lim, Y. Zhang, Bulletin of the Institute of Mathematics, Academia Sinica 2 (2007) 495.
[24] S.M. Chang, W.W. Lin, S.F. Shieh, J. Comput. Phys. 202 (2005) 367.
[25] K. Kasamatsu, M. Tsubota, M. Ueda, Phys. Rev. A 66 (2002) 053606.
[26] U.R. Fischer, G. Baym, Phys. Rev. Lett. 90 (2003) 140402.
[27] G.M. Kavoulakis, G. Baym, New J. Phys. 5 (2003) 51.
[28] W. Bao, I.-L. Chern, F. Lim, J. Comput. Phys. 219 (2006) 836.
[29] L.D. Landau, E.M. Lifschitz, Quantum Mechanics: Non-Relativistic Theory, Pergamon Press, Oxford, 1977.
[30] T. Kuga, Y. Torii, N. Shiokawa, T. Hirano, Y. Shimizu, H. Sasada, Phys. Rev. Lett. 78 (1997) 4713.
[31] A. Aftalion, I. Danaila, Phys. Rev. A 68 (2003) 023603.
[32] Y. Zhang, W. Bao, Appl. Numer. Math. 57 (2007) 697.
[33] T.K. Ghosh, Eur. Phys. J. D 31 (2004) 101.